Journal of Manufacturing Processes xxx (xxxx) xxx–xxx

Contents lists available at ScienceDirect

Journal of Manufacturing Processes

journal homepage: www.elsevier.com/locate/manpro

Study effects of particle size in metal nanoink for electrohydrodynamic inkjet printing through analysis of droplet impact behaviors

Yanhua Huang[a,1], Liangkui Jiang[b,1], Beiwen Li[c], Pavithra Premaratne[d], Shan Jiang[a,*], Hantang Qin[b,*]

[a] Materials Science & Engineering, Iowa State University, Ames, IA, 50011, United States
[b] Industrial & Manufacturing Systems Engineering, Iowa State University, Ames, IA, 50011, United States
[c] Mechanical Engineering, Iowa State University, Ames, IA, 50011, United States
[d] Department of Physics and Engineering, Central College, Pella, IA, 50219, United States

ARTICLE INFO

Keywords:
Electrohydrodynamic inkjet printing
Droplet impact behavior
Particle size
Ink formulation
Metal nanoink

ABSTRACT

Ink properties play a critical role in different printing techniques. However, it is not straightforward to correlate ink properties to the printing results. In this study, several parameters were identified and analyzed to evaluate the droplet behavior in electrohydrodynamic inkjet printing. More specifically, the effects of metallic nanoparticle sizes in the ink formulation were explored through the analysis of droplet impact behaviors. These parameters include droplet wetting diameter, height, initial impact velocity, and contact angle. With the assistance of machine vision, a high-speed camera captured a sequence of images, which were analyzed to extract the aforementioned parameters. Under fields of gravitational force with/without electric force, four phases of ink droplet behaviors were identified. Our data suggest that with an electric force field, particle size dominates the droplet behavior in respect to contact angle and wetting diameter. The increase of particle size decreased the droplet wetting diameter with an electric field, while increased the droplet wetting diameter without the electric field applied. Larger droplet size resulted in higher bouncing frequency and lower droplet height. Furthermore, under both gravitational and electrical fields, the droplet with medium particle size (average diameter of 276 nm) had a higher impact velocity than that with small (average diameter of 140 nm) and big (average diameter of 1517 nm) particle sizes. This study contributes to fundamental understanding of particle size effects. The results will help optimize ink formulations when designing new ink materials for electrohydrodynamic inkjet printing.

1. Introduction

The ability to fabricate Nano/micro scale droplet/wire with functional inks plays key role in a wide range of manufacturing applications such as circuit boards [1], transistors [2], capacitors [3], solar cells [4], new sensor developments [5], flexible electronics development and productions [6]. In order to precisely regulate shape, size, and separation distance perspective of the engineered patterns and droplet arrays fabrication processes, several techniques were developed and optimized, including template-assisted methods [7,8], optical lithography [9,10], and ink-jet printing [11,12]. Optical lithography has been widely used in the industry because of the two to three orders of magnitude higher resolution compared to other approaches [13]. However, it requires expensive equipment, complex chemical reactions, and a time-consuming process, thus limiting this technology to print a circuit board (PCB) manufacturing [14]. The template-assist method provides the flexibility to print multiple materials [15] as well as print on soft flexible substrates such as Polyethylene terephthalate (PET) substrate [16]. It is still limited by the high cost of template fabrication and short life cycle [17]. On the contrary, inkjet printing is a non-contact printing approach that delivers pigments in the form of droplets [18]. Inkjet printing is a bottom-up manufacturing approach that overcomes many obstacles faced by traditional subtractive manufacturing [19] similar to additive manufacturing. Although inkjet printing may not provide the same resolution as optical lithography, its inexpensiveness still attracts a vast amount of industries [20].

There are two major categories of inkjet printing: Drop-On-Demand (DOD) and continuous methods [21]. By eliminating the ink recovery

* Corresponding authors.
E-mail addresses: sjiang1@iastate.edu (S. Jiang), qin@iastate.edu (H. Qin).
[1] Co-first authors.

https://doi.org/10.1016/j.jmapro.2020.04.021
Received 1 December 2019; Received in revised form 19 February 2020; Accepted 11 March 2020

mechanism and improving the efficiency of the ink usage, DOD method has become popular in the industry. Based on the droplet forming physics, DOD ink-jet printing categories into four methods: thermal, electrostatic, piezoelectric, and acoustic [21]. For the thermal method, the inks shall contain highly volatile chemical solvents, so that the heater imbedded in the print head can generate solvent gas bubbles to eject ink out of the ink chamber forming the ink droplet [22]. For the piezoelectric method, droplets are generated by electric potential triggered mechanical deformation of piezoelectric material installed in the ink chamber. The viscosity of the inks was modified by a series of surfactants in order to ensure droplet generation reliability [23]. The electrostatic method utilizes an electric potential applied on the nozzle to generate droplets by providing energy to create new surfaces where droplets separated from ink mainstream. The acoustic method uses mechanical vibrations to generate droplets by resonating ink liquid [24]. Ink formulation for acoustic DOD printing requires modifications to thermodynamic and acoustic behavior in addition to viscosity optimizations [25,26]. Among DOD inkjet printing, electrohydrodynamic (EHD) printing, also known as e-jet printing, possess unique aspects and countless potential applications [27–32]. Lyu, et al. were able to print tungsten nano ink on a flexible substrate to shield x-ray radiation for electronic chips [31]. By combining the advantages of the thermal and electrostatic DOD method, EHD printing requires no volatile chemicals present in its formulation [33], tolerates ink with flexible properties [34].

To better understand the ink properties impacting the printing process, some studies have been conducted to further investigate the correlation between materials properties (density, surface tension, and viscosity) and the printing conditions (nozzle size and ink flow rate). By analyzing high-speed droplet images, Jang et al. found that Ohnesorge number in the range between 4 and 14 provides droplet formability, maximum allowable jetting frequency, and positional accuracy [26]. With different compositions of ethylene glycol, water, and diethylene glycol, fluid's Re, We, and Oh can be engineered with a fixed nozzle diameter and flow rate [26]. Derby reported that with the increase of solid content level, relative viscosity, density will increase, which leads to the decrease of Ohnesorge number [35]. Tai et al. later demonstrated the velocity of ejected droplets was governed by the Ohnesorge numbers [36], in good agreement with Derby and Reis [37].

For metallic inkjet printing, metallic particle size has multiple impacts on ink fluid properties. Typically, ink formulation contains four major components: pigment, which provides color and functions, surfactant which coated the pigment particle surface assisting better dispersion/ suspension, solvent who provide an aqueous environment and flowability, and additives which often improve adhesion, thermal stability, and antibiotics [38]. Einstein-stoke equation reveals the relationships of necessary viscosity of the fluid to suspend different-sized particles [39]. Lee et al. reported that the pigment weight ratio and pigment particle size influenced optical properties (printing result) [40]. Biswas et al. reported that coffee-ring effects increases printed by small pigment particle formulated inks (printing results) [41].

To understand the impact of particle size in the ink formulation during the printing process, we investigated three different particle-size formulated inks droplet behavior under different conditions. Analyzing the captured images from a high-speed camera, four phases were identified. Several parameters, including droplet impact velocity, droplet wetting diameter, droplet height, and contact angle, were extracted from the image for analyzing fluid viscosity, surface tension, and charge capacity properties.

2. Materials and methods

2.1. Materials

Tungsten nano-powder was purchased from US Research Nanomaterials (Houston, TX) and used as received. Other chemicals were purchased from Sigma-Aldrich (St. Louis, MO) unless specified.

2.2. Particle size separation

In a 50-mL centrifuge tube, 2 g of dry tungsten nano-powder was mixed with 40 mL of ethylene glycol with the assistance of vertex and sonication for 30 min. The resulting mixture was centrifuged under 300 rpm for 60 min. Secondly, 5 mL of ethanol was added to the centrifuged supernatant (S1) and precipitate (P1). P1 was homogenized with the assistance of vertex and sonication for 10 min. S1 and P1 were centrifuged under 5000 rpm for 60 min. Resulting supernatant from S1 (S1S2) was further centrifuged down with 10,000 rpm for 10 min, precipitating particles are classified as small particles (average diameter of 140 nm). Resulting precipitate form S1 (S1P2) and resulting supernatant form P1 (P1S2) were centrifuged under 10,000 rpm for 10 min after mixing and 10 min sonication. The resulting precipitate (S1P2-P1S2) P3 was classified as the medium particle (average diameter of 276 nm). The resulting precipitate from P1 (P1P2) was classified as a large particle (average diameter of 1517 nm).

2.3. Ink formulation

The working solution defines as the aqueous solution of the ink except for the pigment. The working solution shall be prepared and homogenized prior to the final mix with the pigment, which is size classified tungsten particle in this study. Based on the function and printing method, working solution properties were optimized accordingly. The working solution was optimized according to several parameters: viscosity, density, evaporation speed, wettability, surface tension.

Triethylene glycol monomethyl ether (TGME) was chosen to be the organic solvent based on its excellent solubility with most hydrophilic liquid and high evaporation rate. Polyvinylpyrrolidone (PVP) is one of the most commonly used metallic nanoparticle surfactants, stabilizers, and adhesive additive in the ink formulation industry [42–46]. With excellent solubility in water and ethanol and low reactivity, PVP was chosen to serve as both surfactant and stabilizer in this study.

2.4. The molecular weight of PVP impacts

For the different molecular weight of PVP, the same concentration water solution, viscosity was increased linearly with the increase of the molecular weight. For e-jet printing, the requirement of viscosity remained at a relatively low level compared to screen printing. Therefore, low molecular PVP was preferred when printing resolution demand was most dominated [47]. However, one of the major disadvantages of low molecular weight PVP surfactants was stability [48,49]. High viscosity commonly provided long stability, therefore, longer shelf life [49,50]. For ink fabrication, small molecular weight and large molecular weight PVP were both facilitated to optimize ink fluid properties.

The concentration of PVP added also impacted the viscosity of the working solution. With sufficient surface coating and stabilization, overall PVP concentration was set at 2 % w/w. To consistently disperse all three sized tungsten particles, the two molecular weights of PVP have been used to facilitate the dispersion [31]. To eliminate the viscosity differences generated by the working solution formulation, all three inks with different particle sizes were formulated using the same working solution.

To prepare a working solution, 1 part (by weight) of PVP 55 K, 1 part of PVP360 K, and 48 parts of TGME were mixed with the assistance of vertex and sonication. In a typical ink formulation process, 50 parts (by weight) of size classified tungsten particle was mixed with 50 parts of pre-mixed working solution, sonicated for 30 min, vertex as much as needed.

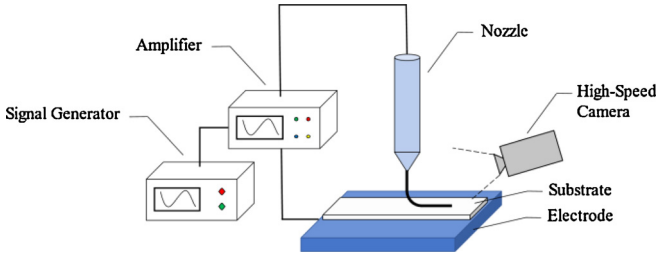

Fig. 1. Schematic diagram of the e-jet printing system.

2.5. E-jet printing system

The e-jet printing system, as shown in Fig. 1, consists of a three-axis stage, a syringe, a nozzle, a signal generator, a voltage amplifier, a glass substrate (75 mm × 20 mm), and a high-speed camera. The voltage was generated, amplified and added between the nozzle and the electrode to provide the desired voltage. The waveform of voltage and related parameters were edited by using a function generator and amplified by a voltage amplifier. The droplets were generated from the tip of the nozzle by an electrical force. The three-axis stage could provide x, y, z movement for fabricating patterns. The motion range of the stage was 160 mm × 160 mm × 250 mm. The precision of the stage was 50 nm. The images of droplets during the printing process were recorded by a high-speed camera (VEO 340 L) with the lens. The images were captured at 8500 frames per second.

Before the printing process, the ink would stay in the nozzle because of surface tension. The electrical field would be applied between the nozzle and electrode when the printing began. With the increase of voltage, the ink would be jetted by electrical force, finally forming Tylor cone at the tip of the nozzle. Then the droplets could generate from the tip of the nozzle because of the Lorentz force. If continuing increasing the voltage, the separate droplets could become a filament.

2.6. Image analysis

The high-speed camera, which could take 8500 frames per second, was used to record the whole printing process. The impact process of the droplet was shown in Fig. 2. The droplet fell under gravity and impacted on the substrate. Increasing the area of the wetted surface and decreasing the overall height of the droplet. After the droplet formed a rectangular shape, the droplet bounced back, and the height of the droplet increased. After achieving the max point, the droplet then expanded for a long time.

Several images of the impact process were analyzed as shown in Fig. 3. Fig. 3a presented the image of the droplet right before contacting the substrate. The diameter of the droplet D_0, the time T_0, and the instantaneous velocity V_0 were measured. Fig. 3b showed the moment that the droplet formed a contact angle of 90 degrees for the first time. In this situation, the height of the droplet, H_1, the diameter of the interface between the droplet and the substrate, D_1, the time T_1, were measured. Fig. 3c presents the moment that the droplet bounced back to the max height. The max height of bounce, H_2, the time, T_2, and the contact angle, θ_0, are measured.

The contact angle formed when the liquid-vapor interface met the liquid-solid interface, and the surface tension of liquid-vapor, liquid-solid, vapor-solid interface achieved a balance. The contact angle is a parameter to qualify the wettability of a solid interface to liquid

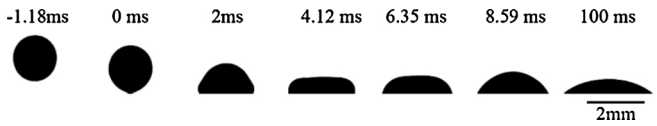

Fig. 2. The image sequence of the droplet impact process.

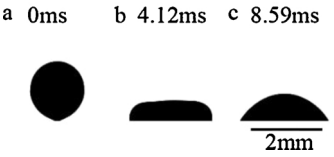

Fig. 3. Images from several significant transition moments.

interface. The initial velocity was calculated by selecting the image with the droplet right before it contacted to the substrate and the last ten figures and calculating the movement of the mass center of the droplet. The velocity could be obtained by dividing the movement of two droplets by time. The changes of diameters of droplets, D, indicates the expedition of droplets when they hit the substrate, which could also reflect the wettability of an ink. The expression is listed below:

$$D = \frac{D_1 - D_0}{D_0} \tag{1}$$

where D was the change of the droplet diameter, D_0 was the diameter of the droplet shown in Fig. 3a. D_1 was the diameter shown in Fig. 3b. The broadest width of the droplet as D_0 at the moment that the droplet contacts the substrate immediately was used as the droplet diameter. D_0 is used to evaluate the size of the droplet. D is the variation of the droplet diameter without the effects of the droplet size.

A particle factorial experiment has been conducted. Under the condition of gravitational force field only, standoff distance was set at 6.3, 8.4, 10.5, and 12.6 mm to mimic the different initial impacting velocity. With both electric force and gravity force present, standoff distance was set at 6.3 mm only to eliminate the velocity difference sourced from gravitational potential. It also eliminated the possible electric field differenced when different voltages were applied. Four different voltages were used in this study to explore the impacts from the electric field. In order to analyze a large number of images and obtain dependable results, a machine vision method based on the MATLAB was applied and optimized [51]. Fig. 4 presented the steps of analysis for extracting information from images. Fig. 4a presented the image extracted by a high-speed camera. Fig. 4b presented the first step, which was finding all edge in the image. As can be seen in Fig. 4b, the edge of the nozzle and the droplet were both extracted (red line). Fig. 4c presented the second step, which was finding the longest edge of the droplet. When the droplet contacted the substrate, its reflection will connect to itself, so the edge of the droplet and its reflection was caught. The third step was to divide this edge into the left part and right part, as shown in Fig. 4d, (left was red, and right was blue). We find the midpoint of the upper edge and divide the whole edge into left and right edges based on the midpoint. The fourth step was to determine the interaction point of the edge and the substrate for each side, as shown in Fig. 4e. The fifth step was to find the contact angle, as shown in Fig. 4f. The tangents of each edge at the interaction point with the substrate were determined. The contact angle was the intersection angle of the tangent and the baseline (the substrate).

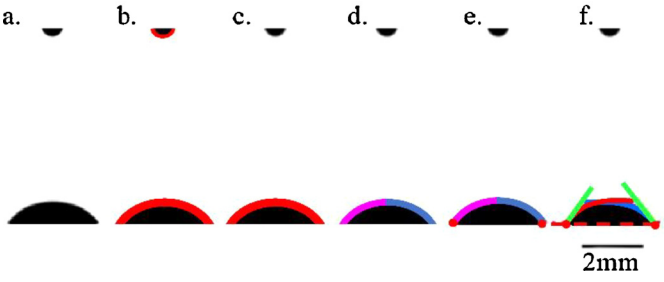

Fig. 4. Steps of image analysis using machine vision, including edge detection, information extraction, and dimensional calculations.

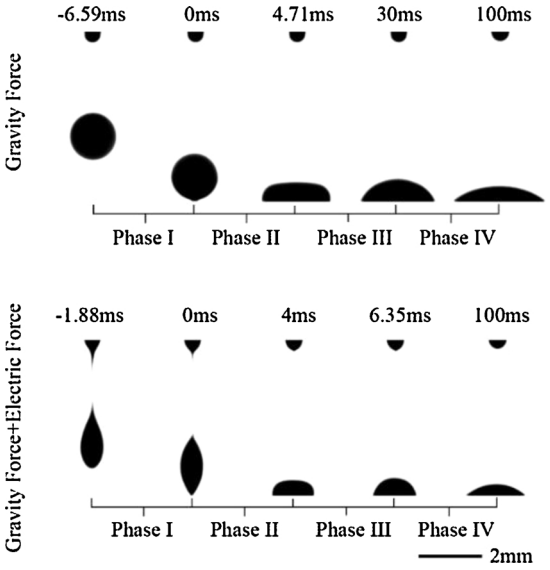

Fig. 5. The different phases during the droplet impact process under the electrical field and the gravitational field.

3. Results and discussion

3.1. The definition of phases

The printing process contains four phases, as shown in Fig. 5. The first phase was before the droplet hits the substrate. Under the lower intensity of the electrical field, the droplet could be close to the cycle when it falls from the nozzle. At the time that the droplet was close to the substrate, the bottom of the droplet could form a bump. With the increase of the electrical field, the shape of the droplet would become thinner and longer. The second phase was from droplets contact the substrate to the time that the droplets from a rectangular for the first time. The center of the droplet could contact the substrate, and the contact area would expand to both sides of the droplet. Meanwhile, the height of the droplet would decrease. The top of the droplet would form a shape similar to a triangle. With time progresses, the center height of the droplet would decrease continuously, and the droplet would finally form a rectangular front-section-view. The contact angle between the droplet and the substrate would decrease from the maximum value to 90 degrees. The third phase was from the end of the last frame to the droplet bounces to the highest point for the first time. At the end of the last frame, the rectangular situation, the velocity of the droplet is not equal to zero, so the fluidity of the droplets could result in that the center of the droplet could continue moving down, which makes the center of the droplet form a drop pit. After achieving the lowest point, the center of the droplet could bounce back and move up. The third phase will end at the time that the center of the droplet achieved the highest point for the first time. The contact angle will decrease when the center moves down and increases with the droplet moving up. The diameter, however, would increase all the time. Phase four was after the droplet bounces back to the highest point, which starts at the end of phase three. In this phase, only the droplet would expand on the substrate, leading to an increase of the diameter and the decrease of the height and the decrease of the contact angle for both sides, a slight bounce or no bounce could be detected.

Fig. 6 presented the change of the parameters, including the diameter, the height, and the contact angle, based on the time. As can be seen, the diameter would increase dramatically in phase 2 and increase slightly in phase 3 and 4. The contact angle would decrease dramatically in phase 2 and decrease slightly in phase 3 and 4. The height of the droplet would decrease dramatically in phase 2 and increase with the bounce of the droplet. After achieving the max point, the height would decrease slowly with the expedition of the droplet in phase 4.

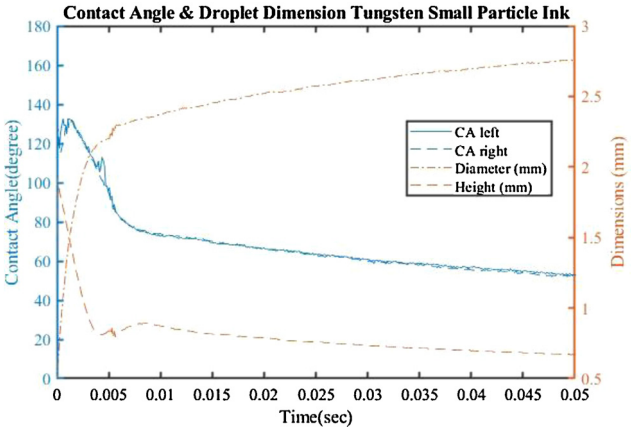

Fig. 6. Time evolution of the contact angle, the diameter and the height of the droplet in the printing process.

3.2. The effects of particle size on droplet impact behaviors

3.2.1. The effects of particle size on the contact angle and wetting diameter

The particle size of tungsten particle impacted on the droplet wetting diameter significantly under the gravitational field only, it did not impact on contact angles at this condition. As shown in Fig. 7a, with the particle size increases, the wetting diameter increases. Commonly, larger particle processes high kinetic energy, which prefers to travel greater than small particles at phase II. This phenomenon indicates that large particle print will result in large dot or wider line width when printing dots or lines, respectively. It does not require denser droplet

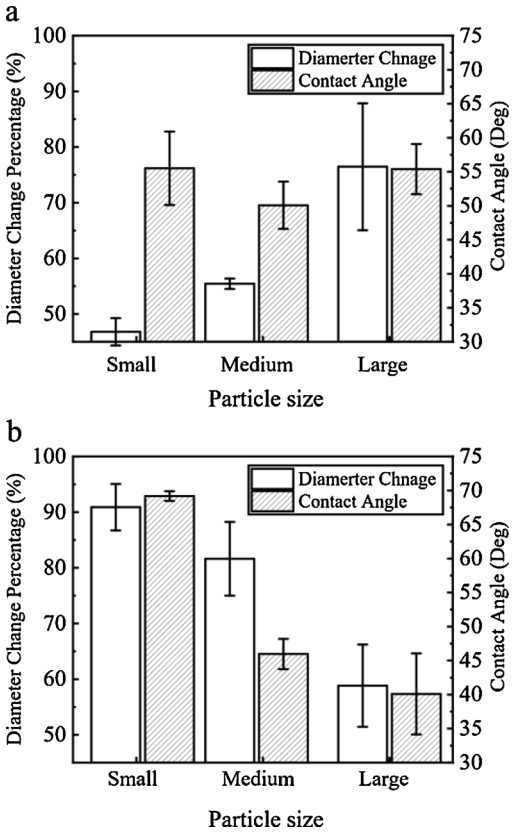

Fig. 7. Contact angle responses to different particle sizes at maximum rebounding and changes of droplet wetting diameters for different particle sizes: (a) without electrical field, and (b) with the electrical field.

separation to form printed lines compare to smaller particle formulated ink.

On the other hand, without the electric potential present, the total energy of the droplet remains constant, which results in constant surface energy across different particle size formulated inks. The contact angle represents surface tension and the surface energy difference between the droplet and substrate. Without different surface energy, no significantly different contact angle response to constant surface energy reasonably.

The particle size of the tungsten particle impacted droplet wetting diameter at the end of phase II and contact angle significantly at the end of phase III with the electric potential present. As shown in Fig. 7b, as particle size increased, from maximum dynamic expansion point to maximum rebounding point, smaller particles formulated ink droplets tended to expand as shown in Fig. 7b. The expansion signified that small particle possesses extra mobility to flow tending for coffee ring effects, on the other hand, large particle tends to settle down, with less coffee ring effects.

On the other aspect, at the end of phase II, kinetic driven droplets expansion ceased, and surface energy and entropy-driven action dominate phase III. With the same tungsten particle mass percentage across different particle size formulated ink, smaller particles formulate ink have greater numbers of particles dispersed in the droplet. It also provides larger total surface areas of particles compare to large size particle formulated ink. Under the assumption of the same charge density per area across all different sized tungsten particles, the total charge on the smaller particles would be greater than the charge on the large particles. This excess charge provides an increase of surface energy, therefore, a larger contact angle.

3.2.2. The effects of particle size on the initial velocity

The initial velocity of the droplet was greatly impacted by the particle size of the tungsten particle when electric field presents. As shown in Fig. 8b with a decrease in particle size, the impact velocity is increased. Similar to expansion, small particles formulated ink possess large particle surface areas where electric charges can accumulate. The large charge provided a large electric force which was the electric field acceleration force, hence the high impact velocity. If the electric field did not present, the gravitational force was the only acceleration force. In Fig. 8a, with initial dropping height increased, the impact velocity increased.

3.2.3. The effects of particle size on the period of the phases

The particle size impacts the phase II duration significantly but not for phase III. As shown in Fig. 9, the duration of phase II (T1) decreased with increases of particle size under both gravitational field only and gravitational-electrical filed conditions. For phase II and phase III duration (T2), T2 decreases when particle size increase without significant difference under gravitational filed only (in Fig. 9a), T2 does not have a linear relationship with particle size for the electrical condition in Fig. 9b.

The particle size impacts the droplet height at both ends of phase II and III ending for both conditions. As shown in both Fig. 9a-b, both H1 and H2 are decreased when the particle size increased. Without electrical fields, small particle formulated ink droplets tend to rebound greatly, by approximate 2.5 times of H2 from the end of phase II to the end of phase III. It was not shown on any other conditions neither particle size variance nor field difference. This may due to greater entropy possessed by smaller particle formulated ink and less field force (gravitational force only with no electric Lorentz force present).

4. Conclusion

In this study, the tungsten nanoparticle inks with three particle sizes (small, medium, large) were prepared and printed using electrohydrodynamic inkjet printing method. The printing process was monitored by using a high-speed camera, and the images were collected and analyzed using a machine vision method. The impact behavior of the droplets was studied, and the main conclusions were listed as the following:

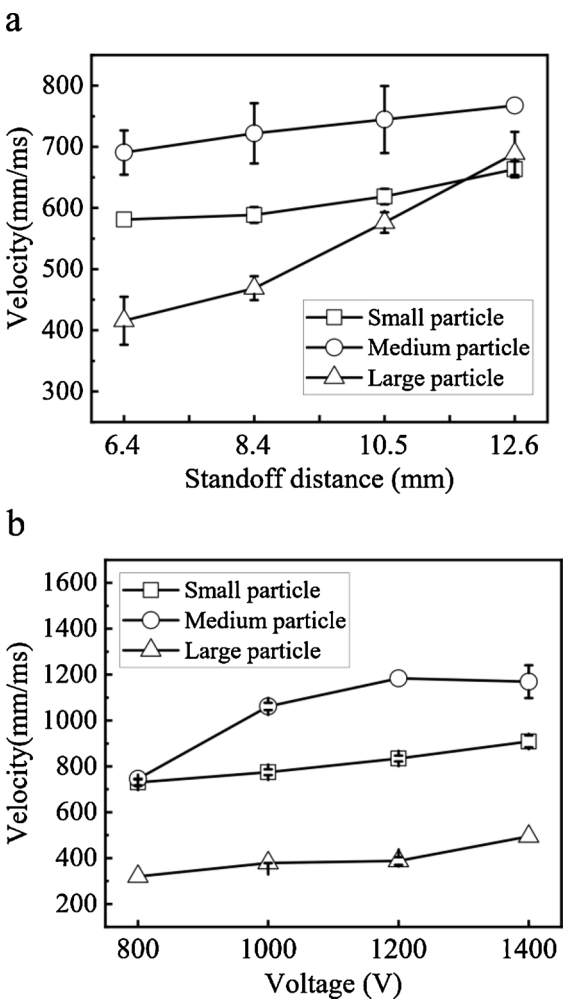

Fig. 8. Initial velocity of the droplet with different particle sizes (a) without and (b) with the electrical field.

- The impact behavior could be clearly identified as four phases: 1) before contact to the substrate, 2) contact the substrate and form a rectangular front-cross-section view, 3) the center of the droplet bounced back, and 4) expansion.
- The phase duration and the height of the droplet increased with the increase of particle sizes under both the gravitational field and the electrical field.
- A larger particle size resulted in a larger diameter under the gravitational field and a smaller diameter under the electrical field.
- The droplets with larger particle size generated smaller contact angles.
- The droplets with medium particle size had the highest impact initial velocity in three particle sizes (small, medium, large).

Declaration of Competing Interest

The patent application of the tungsten nanoink for e-jet printing is currently under review at Office of Intellectual Property and Technology Transfer Office at Iowa State University for US Patent (ISURF #04952). The authors declare that they have no other known competing financial interests or personal relationships that could have

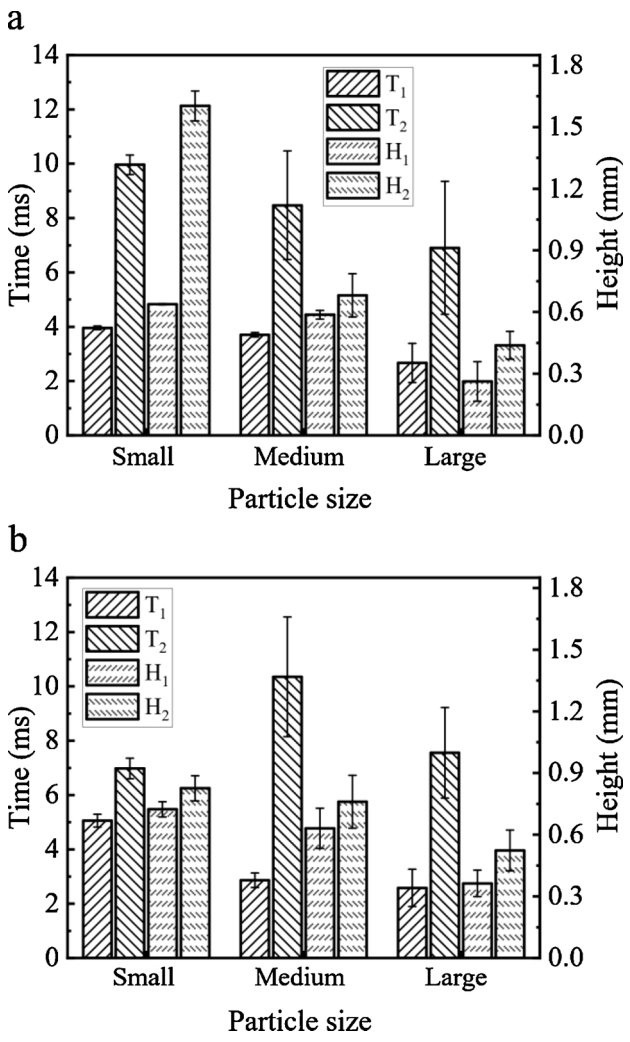

Fig. 9. Time period of phase II and III, and droplet height response to different particles at the end of phase II and III: (a) without and (b) with electrical field applied.

appeared to influence the work reported in this paper.

Acknowledgments

The research is supported by startup accounts of Dr. Jiang and Dr. Qin, and the Undergraduate Research Assistant Program from the Department of Industrial and Manufacturing Systems Engineering (IMSE_URA) at Iowa State University. Dr. Jiang would like to thank 3M for the Non-tenured Faculty Award. We gratefully acknowledge Dr. Fei Liu and Mr. Xiao Zhang for advising on the ink preparation and printing. We also thank the URAs, Kimmo and Vandi Hartanto, for assisting the image analysis.

References

[1] Huang Y, Li W, Qin M, Zhou H, Zhang X, Li F, et al. Printable functional chips based on nanoparticle assembly. Small 2017;13.
[2] Grubb PM, Subbaraman H, Park S, Akinwande D, Chen RT. Inkjet printing of high performance transistors with micron order chemically set gaps. Sci Rep 2017;7.
[3] Worsley R, Pimpolari L, McManus D, Ge N, Ionescu R, Wittkopf JA, et al. All-2D material inkjet-printed capacitors: toward fully printed integrated circuits. ACS Nano 2019;13:54–60.
[4] Stüwe D, Mager D, Biro D, Korvink JG. Inkjet technology for crystalline silicon photovoltaics. Adv Mater 2015;27:599–626.
[5] Downey ARJ, Yan J, Zellner EM, Kraus KH, Rivero IV, Laflamme S. Use of flexible sensor to characterize biomechanics of canine skin. BMC Vet Res 2019;15.
[6] Gao M, Li L, Song Y. Inkjet printing wearable electronic devices. J Mater Chem C 2017;5:2971–93.
[7] Zhang M, Lenhert S, Wang M, Chi L, Lu N, Fuchs H, et al. Regular arrays of copper wires formed by template-assisted electrodeposition. Adv Mater 2004;16:409–13.
[8] Penner RM, Martin CR. Preparation and electrochemical characterization of ultra-microelectrode ensembles. Anal Chem 1987;59:2625–30.
[9] Flavin PG. Physical limitations in lithography for microelectronics. Phys Educ 1981;16:234–8.
[10] Su WX, Wu CY, Lee YC. Anti-reflection nano-structures fabricated on curved surface of glass lens based on metal contact printing lithography. Microelectron Eng 2019;214:15–20.
[11] Karim N, Afroj S, Tan S, Novoselov KS, Yeates SG. All inkjet-printed graphene-silver composite ink on textiles for highly conductive wearable electronics applications. Sci Rep 2019;9.
[12] Chen J, Wise KD. A high-resolution silicon monolithic nozzle array for inkjet printing. IEEE Trans Electron Dev 1997;44:1401–9.
[13] Onses MS, Sutanto E, Ferreira PM, Alleyne AG, Rogers JA. Mechanisms, capabilities, and applications of high-resolution electrohydrodynamic jet printing. Small 2015;11:4237–66.
[14] Kim K, Bae J, Noh SH, Jang J, Kim SH, Park CE. Direct writing and aligning of small-molecule organic semiconductor crystals via “dragging mode” electro-hydrodynamic jet printing for flexible organic field-effect transistor arrays. J Phys Chem Lett 2017;8:5492–500.
[15] Park KS, Baek J, Park Y, Lee L, Lee YEK, Kang Y, et al. Inkjet-assisted nanotransfer printing for large-scale integrated nanopatterns of various single-crystal organic materials. Adv Mater 2016;28:2874–80.
[16] Hyun WJ, Secor EB, Hersam MC, Frisbie CD, Francis LF. High-resolution patterning of graphene by screen printing with a silicon stencil for highly flexible printed electronics. Adv Mater 2015;27:109–15.
[17] Roleček J, Pejchalová L, Martínez-Vázquez FJ, Miranda González P, Salamon D. Bioceramic scaffolds fabrication: indirect 3D printing combined with ice-templating vs. robocasting. J Eur Ceram Soc 2019;39:1595–602.
[18] Derby B. Inkjet printing ceramics: from drops to solid. J Eur Ceram Soc 2011;31:2543–50.
[19] Shirazi SFS, Gharehkhani S, Mehrali M, Yarmand H, Metselaar HSC, Adib Kadri N, et al. A review on powder-based additive manufacturing for tissue engineering: selective laser sintering and inkjet 3D printing. Sci Technol Adv Mater 2015;16.
[20] Zhu J, Li J, Zhong Q, Wang H, Huang L, Fontein F, et al. Lithography compatible, flexible micro-organic light-emitting diodes by template-directed growth. Small Methods 2019;3:1800508.
[21] Le HP. Progress and trends in ink-jet printing technology. 2020. n.d.
[22] Derby B. Additive manufacture of ceramics components by inkjet printing. Engineering 2015;1:113–23.
[23] Di Risio S, Yan N. Piezoelectric ink-jet printing of horseradish peroxidase: effect of ink viscosity modifiers on activity. Macromol Rapid Commun 2007;28:1934–40.
[24] Basak I. Characterisation and comparison of 3D printed and glass moulded optics. Finland: University of Eastern; 2015.
[25] Reis N, Ainsley C, Derby B. Viscosity and acoustic behavior of ceramic suspensions optimized for phase-change ink-jet printing. J Am Ceram Soc 2005;88:802–8.
[26] Jang D, Kim D, Moon J. Influence of fluid physical properties on ink-jet printability. Langmuir 2009;25:2629–35.
[27] Maktabi S, Chiarot PR. Electrohydrodynamic printing of organic polymeric resistors on flat and uneven surfaces. J Appl Phys 2016;120.
[28] Kim Y, Jang S, Oh JH. High-resolution electrohydrodynamic printing of silver nanoparticle ink via commercial hypodermic needles. Appl Phys Lett 2015;106:14103.
[29] Prasetyo FD, Yudistira HT, Nguyen VD. Ag dot morphologies printed using electrohydrodynamic (EHD) jet printing based on a drop-on-demand (DOD). 2020. n.d.
[30] Qin H, Dong J, Lee YS. AC-pulse modulated electrohydrodynamic jet printing and electroless copper deposition for conductive microscale patterning on flexible insulating substrates. Robot Comput Integr Manuf 2017;43:179–87.
[31] Lyu H, Zhang X, Liu F, Huang Y, Zhang Z, Jiang S, et al. Fabrication of micro-scale radiation shielding structures using tungsten nanoink through electrohydrodynamic inkjet printing. J Micromech Microeng 2019;29:115004.
[32] Zhang X, Lies B, Lyu H, Qin H. In-situ monitoring of electrohydrodynamic inkjet printing via scalar diffraction for printed droplets. J Manuf Syst 2019;53:1–10.
[33] Cui Z, Han Y, Huang Q, Dong J, Zhu Y. Electrohydrodynamic printing of silver nanowires for flexible and stretchable electronics. Nanoscale 2018;10:6806.
[34] Sharma A, Bakis CE, Wang KW. The effect of electrostatic and electrohydrodynamic forces on the chaining of carbon nanofibres in liquid epoxy. J Phys D Appl Phys 2010;43.
[35] Derby B. Inkjet printing of functional and structural materials: fluid property requirements, feature stability, and resolution. 2010.
[36] Tai J, Gan HY, Liang YN, Lok BK. Control of droplet formation in inkjet printing using ohnesorge number category: materials and processes. 10th Electron. Packag. Technol. Conf. EPTC 2008 2008:761–6.
[37] Derby B, Reis N. Inkjet printing of highly loaded particulate suspensions. MRS Bull 2003;28:815–8.
[38] Poole CF. Instrumental thin-layer chromatography. Elsevier Inc.; 2014.
[39] Einstein A. Über die von der molekularkinetischen Theorie der Wärme geforderte Bewegung von in ruhenden Flüssigkeiten suspendierten Teilchen. Ann Phys 1905;322:549–60.
[40] Lee H-K, Joyce MK, Fleming PD. Influence of pigment particle size and pigment ratio on printability of glossy ink jet paper coatings. 2020. n.d.
[41] Biswas S, Gawande S, Bromberg V, Sun Y. Effects of particle size and substrate surface properties on deposition dynamics of inkjet-printed colloidal drops for printable photovoltaics fabrication. J Sol Energy Eng Trans ASME

2010;132:0210101–7.
[42] Tung H-T, Chen I-G, Kempson IM, Song J-M, Liu Y-F, Chen P-W, et al. Shape-controlled synthesis of silver nanocrystals by X-ray irradiation for inkjet printing. 2012.
[43] Xiong Y, Washio I, Chen J, Cai H, Li Z-Y, Xia Y. Poly(vinyl pyrrolidone): a dual functional reductant and stabilizer for the facile synthesis of noble metal nanoplates in aqueous solutions. 2006.
[44] Chien Dang M, My Dung Dang T, Fribourg-Blanc - E, Thu Tuyet Le T, Fribourg-Blanc E, et al. Silver nanoparticles ink synthesis for conductive patterns fabrication using inkjet printing technology. Adv Nat Sci Nanosci Nanotechnol 2015;6:15003.
[45] Howe KS, Clark ER, Bowen J, Kendall K. A novel water-based cathode ink formulation. Int J Hydrogen Energy 2013;38:1731–6.
[46] Romih T, Jemec A, Kos M, Hočevar SB, Kralj S, Makovec D, et al. The role of PVP in the bioavailability of Ag from the PVP-stabilized Ag nanoparticle suspension. Environ Pollut 2016;218:957–64.
[47] Chien Dang M, Dung Dang TM, Fribourg-Blanc E. Silver nanoparticles ink synthesis for conductive patterns fabrication using inkjet printing technology. Adv Nat Sci Nanosci Nanotechnol 2015;6. Institute of Physics Publishing.
[48] Jang E, Kim E, Son HY, Lim EK, Lee H, Choi Y, et al. Nanovesicle-mediated systemic delivery of microRNA-34a for CD44 overexpressing gastric cancer stem cell therapy. Biomaterials 2016;105:12–24.
[49] Khondoker MAH, Mun SC, Kim J. Synthesis and characterization of conductive silver ink for electrode printing on cellulose film. Appl Phys A Mater Sci Process 2013;112:411–8.
[50] Omastová M, Bober P, Morávková Z, Peřinka N, Kaplanová M, Syrový T, et al. Towards conducting inks: polypyrrole-silver colloids. Electrochim Acta 2014;122:296–302.
[51] Drop shape analysis. Fit contact angle by double ellipses or polynomials - File Exchange - MATLAB Central. 2020. n.d.